







Article

Zipserite, a new bismuth chalcogenide $\text{Bi}_5(\text{S,Se})_4$ from Nagybörzsöny in Hungary with a $R\bar{3}m(00\gamma)00$ modulated structure

Juraj Majzlan¹ , Daniel Ozdín², Jiří Sejkora³ , Gwladys Steciuk⁴, Jakub Plášil⁴ , Christiane Rößler⁵  and Christian Matthes⁵

¹Institute of Geosciences, Friedrich-Schiller University, Burgweg 11, 07749 Jena, Germany; ²Department of Mineralogy, Petrology and Economic Geology, Faculty of Natural Sciences, Comenius University, Ilkovičova 6, 842 15 Bratislava, Slovakia; ³Department of Mineralogy and Petrology, National Museum, Cirkusová 1740, 193 00 Praha 9-Horní Počernice, Czech Republic; ⁴Institute of Physics of the CAS, Na Slovance 2, 182 21 Praha 8, Czech Republic; and ⁵Bauhaus University, Coudraystrasse 11, 99423 Weimar, Germany

Abstract

Zipserite is a new mineral species discovered in a sample collected from the old mine dumps of the abandoned epithermal deposit Nagybörzsöny in Hungary. Zipserite occurs as anhedral to subhedral, lath-like grains, up to 500 μm in size, in hydrothermally strongly altered rocks. It is found at a contact between bismuth and bismuthinite, also associated with rare ikonolite and joséite-A. Zipserite is silvery white with a metallic lustre. Mohs hardness is ca. 2–3 and the calculated density is $7.815 \text{ g}\cdot\text{cm}^{-3}$. In reflected light, zipserite is grey–white, with colour and reflectance essentially matching those of bismuthinite. Bireflectance is weak, internal reflections not present. Anisotropy is moderately strong, with dark blue and grey colours of anisotropy. Reflectance values for the four Commission on Ore Mineralogy wavelengths of zipserite in air [R_{max} , R_{min} (%) (λ in nm)] are: 48.4, 46.4 (470); 47.8, 45.9 (546); 47.8, 45.8 (589); and 47.5, 45.6 (650). The empirical formula, based on electron-microprobe analyses, is $(\text{Bi}_{4.74}\text{Pb}_{0.31})_{\Sigma 5.05}(\text{S}_{3.38}\text{Se}_{0.56}\text{Te}_{0.02})_{\Sigma 3.96}$, that can be simplified as $\text{Bi}_5(\text{S,Se})_4$. The ideal end-member formula of zipserite is Bi_5S_4 , which requires Bi 89.07 and S 10.93, total 100 wt.%. Zipserite possesses a fascinating crystal structure. The average structure is trigonal, with space group $P\bar{3}m$, $a = 4.162(1) \text{ \AA}$, $c = 16.397(1) \text{ \AA}$, $V = 245.94(4) \text{ \AA}^3$ and $Z = 2$. The structure is built by the alternation of a double bismuth layer Bi_2 and the Bi_3S_4 block which is a three octahedra thick layer. Its general formula can be expressed as $\text{Bi}_2 + \text{Bi}_3\text{S}_4$, which corresponds directly to the observed stacking. At 98 K, the structure can be described using the superspace formalism with an R -centred trigonal unit cell $a = 4.209(2) \text{ \AA}$, $c_0 = 5.616(6) \text{ \AA}$, a modulation vector $\mathbf{q} \approx 4/3 \mathbf{c}^*$ and the superspace group $R\bar{3}m(00\gamma)00$. Zipserite is not only a new mineral but also the first named member of a new sub-group of compounds within the broader family of bismuth chalcogenides, characterised by complex stacking of structural units (Bi_2 layers and Bi_3S_4 blocks). Some of these phases are being investigated as promising thermoelectric materials and synthetic analogues of zipserite could also be inspected for similar physical properties.

Keywords: zipserite; new mineral; bismuth sulfide; modulated structure

(Received 8 February 2024; accepted 25 April 2024; Accepted Manuscript published online: 3 May 2024)

Introduction

Bismuth chalcogenides are long known for their pronounced degree of metallic bonding in their structures, a prominent example thereof being tetradymite, $\text{Bi}_2\text{Te}_2\text{S}$ (Pauling, 1975). They are the subject of intensive interest in materials science, with the ‘archetypal tetradymites’ Bi_2Se_3 , Bi_2Te_3 and Sb_2Te_3 (Cook *et al.*, 2007; Heremans *et al.*, 2017). The tetradymites (in the materials-science sense) are one of the most promising groups of thermoelectric materials, designed to convert waste heat into electricity (Yamini *et al.*, 2023). Tuning of the properties, either *via* variations in the elemental ratios or modification of crystal structures, could

enhance the thermoelectric effect and lead to greater applicability (Pathak *et al.*, 2022). The discovery of new crystal structures of this type, however, is not restricted to the chemical laboratories. New sulfide phases are being reported from Nature, some with previously known and some with novel structures (Kuribayashi *et al.*, 2019; Bindi *et al.*, 2023; Sejkora *et al.*, 2023a, 2023b). The description of new minerals from this group of phases could inspire the development of thermoelectric materials.

In this work, we are reporting the properties and crystal structure of a new bismuth chalcogenide discovered in Nature. Its mineral assemblage and mode of occurrence suggest how it could be prepared in the laboratory and this phase could be of interest for novel types of thermoelectric materials. The modulated crystal structure can be rationalised and compared to other chemically related phases in the bismuth–sulfide system. The new mineral, zipserite, and its symbol *zps* were approved by the Commission on New Minerals, Nomenclature and Classification of the International Mineralogical Association (IMA2022–075, Majzlan *et al.*, 2022).

Corresponding author: Juraj Majzlan; Email: Juraj.Majzlan@uni-jena.de

Associate Editor: Owen Missen

Cite this article: Majzlan J., Ozdín D., Sejkora J., Steciuk G., Plášil J., Rößler C. and Matthes C. (2024) Zipserite, a new bismuth chalcogenide $\text{Bi}_5(\text{S,Se})_4$ from Nagybörzsöny in Hungary with a $R\bar{3}m(00\gamma)00$ modulated structure. *Mineralogical Magazine* 88, 482–492. <https://doi.org/10.1180/mgm.2024.37>

© The Author(s), 2024. Published by Cambridge University Press on behalf of The Mineralogical Society of the United Kingdom and Ireland. This is an Open Access article, distributed under the terms of the Creative Commons Attribution licence (<http://creativecommons.org/licenses/by/4.0/>), which permits unrestricted re-use, distribution and reproduction, provided the original article is properly cited.

The name zipserite honours Kristián Andrej (or also Christian Andreas) Zipser (born November 25, 1783, Győr, Hungary, died February 20, 1864, Banská Bystrica, Slovakia), a prominent mineralogist of the Austro-Hungarian Empire in the 19th Century. He contributed significantly to the establishment of the second oldest Mineralogical Society in the world (1811, Banská Štiavnica, Slovakia), which is followed by today's Slovak Mineralogical Society. Zipser was a member of more than 80 scientific societies and museums and an honorary doctor of several European universities. For his activities, Zipser gained great authority throughout Europe, resulting in several foreign orders and awards from European emperors, kings and dukes. He collected many hand specimens of minerals, which he sent free of charge to museums, universities, institutes, scientists and monarchs, thus significantly enriching the collections of institutions in almost all countries in Europe and North America.

The holotype material (polished section) is deposited in the Mineralogical Museum of Comenius University, Faculty of Natural Sciences in Bratislava, Slovakia, under catalogue number MMUK 7670.

Occurrence and mineral description

Occurrence

Zipserite was found in samples with bismuth sulfotellurides, taken from the tailings pile of the Alsó-Rózsa adit, ~5 km ENE of the village Nagybörzsöny in Hungary (GPS coordinates: 47° 56'27"N, 18°53'40"E). Hydrothermal base-metal and precious metal mineralisation are developed in this deposit in andesites to dacites of Miocene age, and are related to the asthenospheric upwelling and subduction of the European platform under the African plate during the last stages of the convergent Alpine collision (Bezák *et al.*, 2023; Hurai *et al.*, 2023). The mineralisation forms veins in andesitic rocks but changes to veinlet zones and disseminations in dacites. The dump material is formed by intensively hydrothermally altered volcanic rocks. The main alteration is propylitisation, which results in the original rocks being changed into a mixture of predominantly white sheet silicates with disseminated sulfides and sulfosalts. Two stages of mineralisation were distinguished: the first stage is represented by pyrite, galena, sphalerite, chalcopyrite and pyrrhotite, and the second one

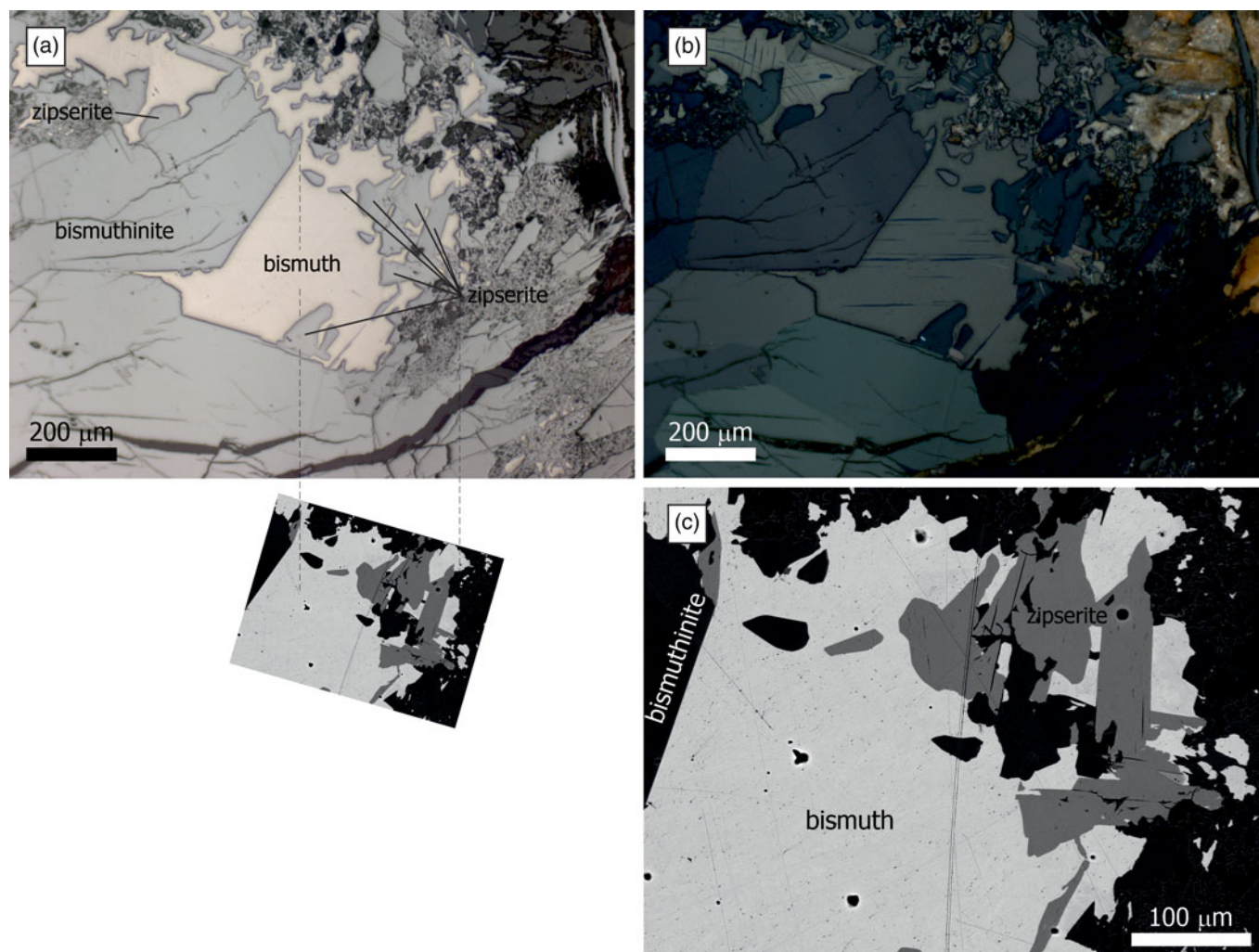


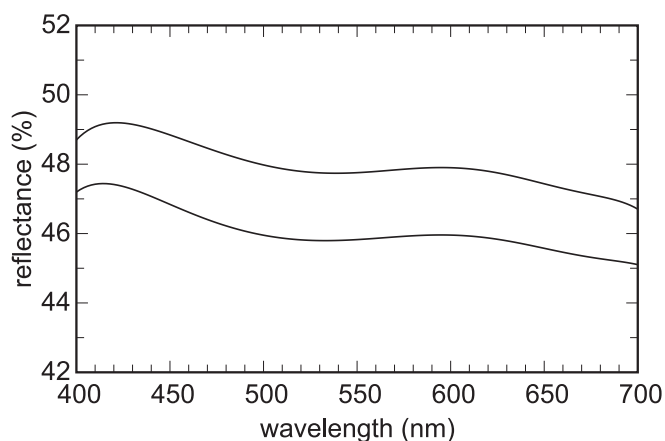
Figure 1. Optical and back-scattered electron (BSE) images of the assemblage of bismuth minerals from Nagybörzsöny, Hungary. (a) Reflected light, one Nicol. Note that the reflectance and colour of zipserite and bismuthinite are very similar. A small BSE image was adjusted to match the orientation and size of the reflected-light image. The dashed lines are guides for the eye. (b) Reflected light, partially crossed Nicols, the same area as shown in (a). Note the dark blue colours of the anisotropy of zipserite. (c) BSE image of the intergrowth of native bismuth, bismuthinite and zipserite. The same image (zoomed out, rotated) was also used in (a). The section used is #AR2-3e, the holotype material, deposited under the catalogue number MMUK 7670 at the Comenius University in Bratislava.

Table 1. Reflectance values for zipserite. The Committee on Ore Minerals (COM) standard wavelengths are given in bold.

R_{\min} (%)	R_{\max} (%)	λ (nm)	R_{\min} (%)	R_{\max} (%)	λ (nm)
47.2	48.7	400	45.9	47.9	560
47.4	49.2	420	46.0	47.9	580
47.1	49.0	440	45.8	47.8	589
46.6	48.7	460	46.0	47.9	600
46.4	48.4	470	45.9	47.8	620
46.2	48.3	480	45.7	47.6	640
46.0	48.0	500	45.6	47.5	650
45.8	47.8	520	45.4	47.2	660
45.7	47.6	540	45.3	47.1	680
45.9	47.8	546	45.1	46.7	700

mainly by arsenopyrite, bismuth, bismuthinite, sulfosalts, gold, baryte and carbonates. Of the various selenium tellurides, the tetradymite minerals pilsenite, ikonolite, tetradymite, joséite-A and joséite-B are present, in addition to other Au–Ag–Bi–Te minerals (jonassonite, petzite, hessite and jaszczakite) (Koch and Grassely, 1952; Paar *et al.*, 2006; Pantó and Mikó, 1964; Szakáll, 2002). Szakáll *et al.* (2012) described “unusual ikonolite” from Nagyborzsöny. Its composition, normalised to 4 S atoms, is $\text{Bi}_{5.29}\text{S}_4$ and $\text{Bi}_{5.12}\text{S}_4$. The structural data were obtained by powder X-ray diffraction, but, given the great degree of similarity among the various Bi–S phases, the “unusual ikonolite” could have actually been zipserite.

The specimens that contain zipserite also contain abundant bismuthinite and native bismuth (Fig. 1) and rare ikonolite and joséite-A. Zipserite is located particularly along the contact between bismuth and bismuthinite, suggesting that it may be a reaction product of these two minerals. Textural evidence suggests that bismuth was the first mineral in the association, and later fluids that brought both Bi and S attacked the early bismuth, and produced zipserite locally. The composition of the altered rocks was not investigated in detail. A peculiar property of these rocks, when embedded in epoxy and prepared as polished sections, is that the rocks expand and crack the sections within a few years. We assume that the altered rocks contain a substantial fraction of smectites that pick up humidity from the air and expand.

**Figure 2.** Smoothed dispersion curves for zipserite. The reflectance values are listed in Table 1.**Table 2.** Electron-microprobe analyses for zipserite. All data in wt.%. S.D. – standard deviation

Element	Mean	Range	S.D.	Standard, emission line
Bi	81.75	80.11–82.97	0.99	Bi_2Se_3 , $M\alpha$
Sb	0.01	0.00–0.04	0.01	Sb_2Te_3 , $L\alpha$
Pb	5.31	4.20–6.37	0.73	PbS , $M\alpha$
Cu	0.01	0.00–0.04	0.02	CuFeS_2 , $K\alpha$
S	8.94	8.01–9.73	0.63	FeS_2 , $K\alpha$
Se	3.64	2.08–5.40	1.21	Bi_2Se_3 , $L\alpha$
Te	0.16	0.04–0.36	0.11	Sb_2Te_3 , $L\alpha$
Total	99.82	99.36–100.06	0.22	

S.D. – standard deviation

Physical and optical properties

Zipserite forms large (up to 500 μm) inclusions in aggregates of bismuth and bismuthinite (Fig. 1). Some of these inclusions seem to be subhedral, lath-like crystals. The colour is silvery, identical to the colour of bismuthinite. Zipserite has a metallic lustre. Hardness is low, estimated as 2–2½, similar to bismuthinite, based on no difference in polishing hardness observed in reflected light. Neither cleavage nor parting was observed owing to the small size of the grains and their intergrowth with other Bi minerals. Density calculated from crystallographic data and empirical formula (see below) is 7.815 $\text{g}\cdot\text{cm}^{-3}$. Attempts to extract zipserite grains for X-ray diffraction (XRD) experiments failed. The mineral appears to be ductile; upon contact with a steel needle, it does not break but produces bent flakes. When subjected to XRD investigation, the results were invariably of poor quality, suggesting that scraping of the material deforms its internal structure.

In reflected light, zipserite has a greyish-white colour (Fig. 1a). Colour and reflectance are essentially indistinguishable from those of the host bismuthinite, making the mineral very difficult to differentiate from bismuthinite. Bireflectance is weak, with creamy white to grey–white colours. Zipserite has no pleochroism and moderately strong anisotropy. The colours of anisotropy are dark blue and grey (Fig. 1b). Zipserite has no internal reflections. Reflectance values (WTiC Zeiss 370) were measured in air (spectrophotometer MSP400 Tidas at Leica microscope, objective 20 \times). They are listed in Table 1 (COM standard wavelengths are given in bold) and shown in Fig. 2.

Chemical composition

Because of the differences in the average atomic number, zipserite can be much more easily differentiated from bismuthinite in back-scattered electron images (Fig. 1c). Quantitative chemical analyses (Table 2) on selected zipserite grains were carried out using a Jeol JXA 8530 electron microprobe (wavelength dispersive spectroscopy mode, 20 kV, 20 nA and 5 μm beam diameter, 20 s on the peak, 20 s on background) at the Department of Mineralogy at the Friedrich Schiller University in Jena. The estimated detection limits (in wt.%) were 0.01 for S, 0.03 for Fe and Cu, 0.06 for Sb, 0.07 for Se and Te, and 0.08 for Pb and Bi. Results (average of 10 spot analyses) are given in Table 2. Contents of other elements with atomic numbers >8 are below detection limits. Matrix correction by ZAF software was applied to the data. The empirical formula calculated on the basis of 9 apfu is $(\text{Bi}_{4.74}\text{Pb}_{0.31})_{\Sigma 5.05}(\text{S}_{3.38}\text{Se}_{0.56}\text{Te}_{0.02})_{\Sigma 3.96}$, the idealised formula can be written as $\text{Bi}_5(\text{S,Se})_4$. The ideal end-member formula of zipserite is Bi_5S_4 , which requires Bi 89.07 and S 10.93, total 100 wt.%.

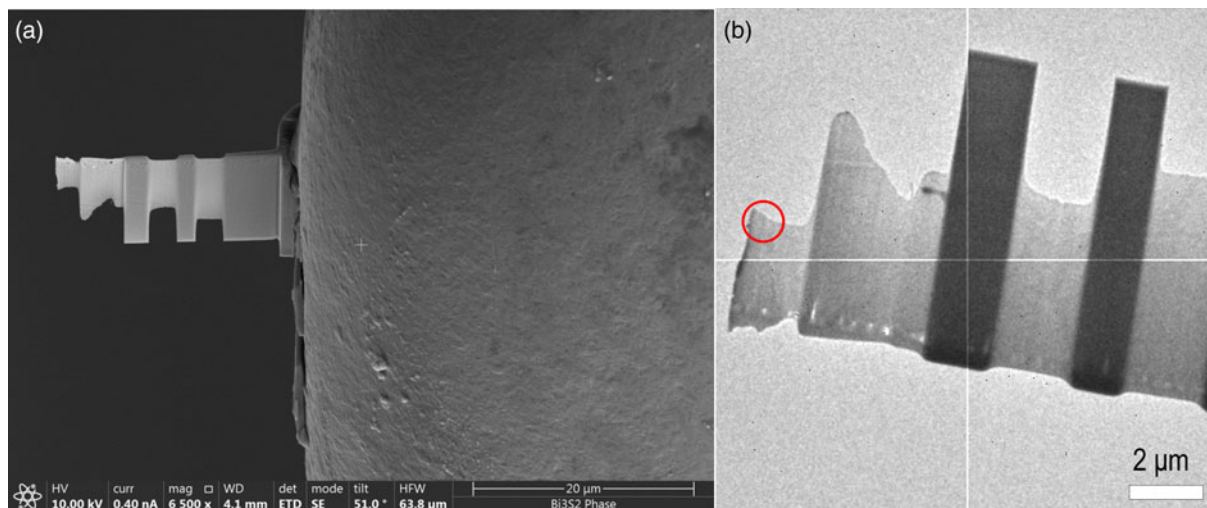


Figure 3. (a) SEM image of the lamella prepared from the $\text{Bi}_5(\text{S,Se})_4$ phase. (b) TEM picture of lamellae and the area selected (red circle) for the 3D ED data collection at 98 K.

Table 3. cRED data collection and structure refinement details for $\text{Bi}_5(\text{S,Se})_4$.

Crystal data	98 K	$\text{Bi}_{1.667}(\text{S}_{1.133}\text{Se}_{0.2})\Sigma_{1.333}$ trigonal	298 K (ambient)
Refined structural formula			
System			
Temperature	98 K		298 K (ambient)
<i>a</i>	4.209(2) Å		4.367(3)
<i>c</i>	5.610(6) Å		5.797(5)
<i>V</i>	86.01(1) Å ³		95.74(12) Å ³
γ from $\mathbf{q} = \gamma\mathbf{c}^*$	1.325(5)		1.330(2)
<i>Z</i>	1		1
Density [g·cm ⁻³]	7.7306		6.9450
Space group		$R\bar{3}m1(00\gamma)00$	
TEM		FEI Tecnai G2 20	
Measurement method		Continuous rotation 3D ED	
Radiation (wavelength)		electrons (0.0251 Å)	
$\Delta\alpha/\text{total } \alpha\text{-tilt } (^\circ)$	0.25/105		0.50/105
Resolution range (θ)	0.04–1.16		0.04–1.16
Limiting Miller indices	<i>h</i> : -5→0, <i>k</i> : 1→5, <i>l</i> : 0→9, <i>m</i> : -2→2		<i>h</i> : -5→0, <i>k</i> : 1→6, <i>l</i> : 0→10, <i>m</i> : -2→2
Number of independent reflections (obs/all) – kinematic	163/163		171/204
R_{int} (obs/all) – kinematic	0.1370/0.1370		0.2082/0.2086
Redundancy	6.344		4.809
Coverage for $\sin\theta/\lambda = 0.7 \text{ \AA}^{-1}$	81.91%		92.58%
Kinematical refinement			
Number of reflections (obs/all)	96/96		104/122
<i>R</i> , <i>wR</i> (obs);	<i>main</i> : 0.1490/0.1636 <i>order 1</i> : 0.1241/0.1531		<i>main</i> : 0.1719/0.2243 <i>order 1</i> : 0.1171/0.1341
<i>R</i> , <i>wR</i> (all);	<i>main</i> : 0.1490/0.1636 <i>order 1</i> : 0.1241/0.1531		<i>main</i> : 0.1723/0.2240 <i>order 1</i> : 0.1259/0.1366
<i>N</i> refined parameters	6		6
Dynamical refinement			
OVF: $\Delta\alpha_v$ /step between OVFs(°)	2.75°/1.75°		3°/2°
Reflection selection criteria $R\text{Sg}(\text{max})$	0.95		1.00
Outliers $ F_{\text{obs}} - F_{\text{calc}} > 30\sigma(F_{\text{obs}})$	24		6
Number of reflections (obs/all)	768/770		616/683
<i>R</i> , <i>wR</i> (obs)	all: 0.0960/0.1185 main: 0.0838/0.1058 order 1: 0.1080/0.1291		all: 0.1142/0.1376 main: 0.1060/0.1419 order 1: 0.1243/0.1318
<i>R</i> , <i>wR</i> (all)	all: 0.0960/0.1185 main: 0.0838/0.1058 order 1: 0.1080/0.1291		all: 0.1192/0.1380 main: 0.1066/0.1420 order 1: 0.1342/0.1327
GOF(obs)/GOD(all)	0.0853/0.0852		0.0721/0.0687
<i>N</i> refined parameters: all/structural	60/6		47/6
Effective thicknesses; variation model	167(6) Å; wedge		201(9); wedge

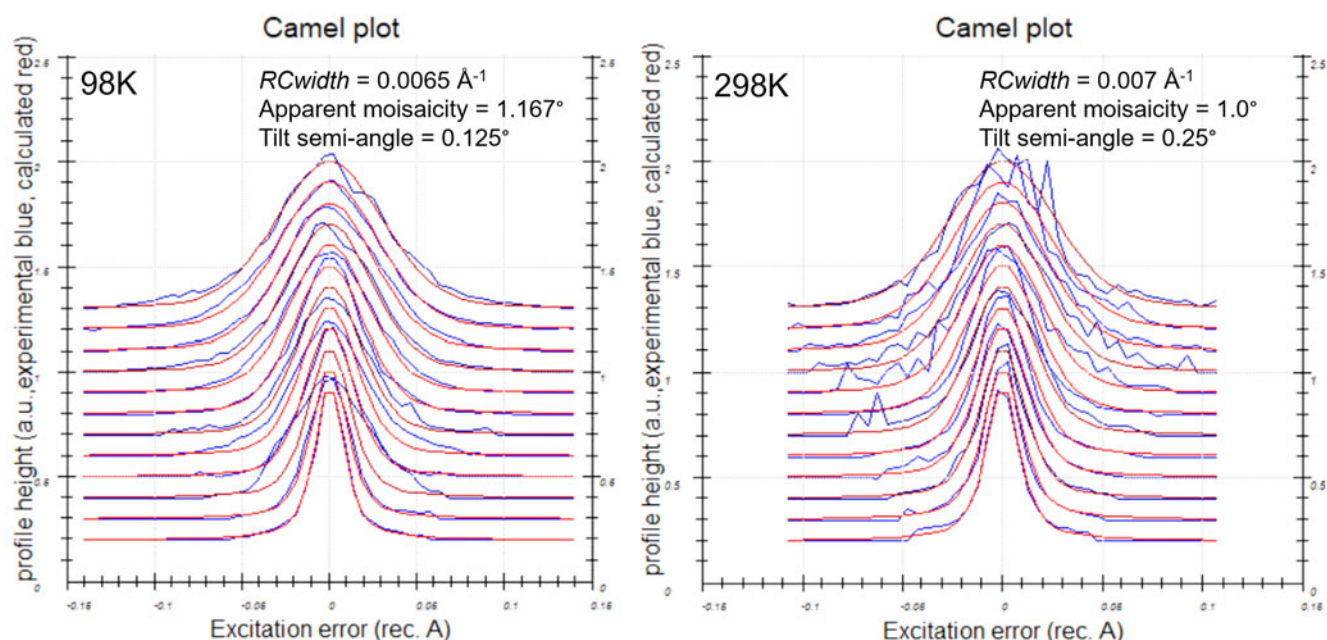


Figure 4. Plots of the rocking-curve profiles (Camel plot) of the experimental 3D ED data at 98 K and 298 K. The lowest blue curve is the averaged observed rocking curve in the range of 0.2 to 0.3 \AA^{-1} and the next ones are obtained by steps of 0.1 \AA^{-1} . The red curves are the calculated ones from the three parameters *Rocking curve width*, *apparent mosaicity* and *tilt semi-angle*. Reflections are involved in the Camel plot for $l > 10\sigma(l)$.

Crystal structure

As mentioned above, attempts to extract a grain for XRD analysis invariably failed. All the flakes extracted were unsuitable for structural characterisation. Therefore, we opted for the structure solution employing electron diffraction, which can easily collect data on a lamella at the nanoscale.

Slicing and polishing of a lamella for 3-dimensional electron diffraction analysis were carried out using a scanning electron microscope (SEM) coupled with a gallium-focused ion beam (FIB) source. The SEM–FIB (Helios G4 UX, ThermoFisherScientific) is equipped with a high-performance FIB source (Phoenix) that allows the polishing of transmission electron microscope (TEM) lamella at very low acceleration voltage or beam current. This feature is essential for obtaining undisturbed thin lamella suitable for high-resolution TEM imaging. Thin sections of samples, as used for optical-light microscopic investigation and other analyses, were sputtered with an $\approx 8 \text{ nm}$ gold layer to ensure the electric conductivity of the full sample and to reduce sample abrasion during ion beam imaging. Sites for extraction of the lamellae were selected according to previous microscopic and spectroscopic characterisation of the samples. Areas of interest were covered with an $\sim 15 \times 15 \times 3 \text{ \mu m}$ layer of platinum to further protect the sample surface against ion beam damage.

The structure analyses were carried out at 98 K and at the ambient temperature (298 K) using the 3-dimensional electron diffraction (3D ED) technique (Gemmi and Lanza, 2019; Gemmi *et al.*, 2019). The first data collection was carried out at low temperature to prevent beam-induced damage and to test the stability of the studied compound under the beam. The 3D ED data were collected on the thinnest part of the lamella (Fig. 3a), with a continuous rotation mode in a FEI Tecnai 02 transmission electron microscope (acceleration voltage of 200 kV, LaB₆) equipped with a side-mounted hybrid single-electron detector ASI Cheetah M3, 512×512 pixels with high sensitivity

and fast readout. A series of non-oriented patterns were collected continuously by steps of 0.25° (98 K) and 0.5° (298 K) on the accessible tilt range allowed by the preparation. The area of the lamella where data were collected is defined by the size of the 1 \mu m beam (nano diffraction mode) (Fig. 3b). Continuous-rotation 3D ED data (cRED) reduction was performed using the computer program *PETS2* (Palatinus *et al.*, 2019; Brázda *et al.*, 2022). The specific data processing for cRED data used in the structure solution and the refinement is detailed extensively in Klar *et al.* (2023). It includes *overlapping virtual frames* (OVFs) for the dynamical refinement that aims to model experimental intensities from continuous rotation data by summing consecutive experimental diffraction patterns into a set of virtual frames (see experimental details in Table 3). Data collected on zipserite show very broad reflections for both temperatures. It leads to very high values of *Rocking curve width* = 0.0065 \AA^{-1} (98 K), and 0.007 \AA^{-1} (298 K), and *apparent mosaicity* = 1.167° (98 K) and 1° (298 K), which affects the accuracy of the refined model (Fig. 4). The data reduction for the structure solution leads to an *hkl*-type file with $R_{int}(\text{obs/all}) = 0.1370/0.1370$ and 81.91% coverage, and $R_{int}(\text{obs/all}) = 0.2082/0.2086$ and 91.58% coverage for $\sin\theta/\lambda = 0.7 \text{ \AA}^{-1}$ (Laue class $\bar{3}m$) for the data collected at 98 K and 298 K, respectively. For the dynamical refinement, another *hkl*-type file is generated where each *OVF* is independently refined (Palatinus *et al.*, 2015a, 2015b; Klar *et al.*, 2023). The structure was solved using *Superflip* (Palatinus and Chapuis, 2007; Palatinus, 2013) in *Jana2020* (Petříček *et al.*, 2023) and refined using *DYNGO* and *Jana2020* (Petříček *et al.*, 2023).

At 98 K, the structure is described using the superspace formalism with a *R*-centred trigonal unit cell of $a = 4.209(2) \text{ \AA}$ and $c_0 = 5.616(6) \text{ \AA}$, a modulation vector $\mathbf{q} \approx 4/3 \mathbf{c}^*$ and, the superspace group $R\bar{3}m(00\gamma)00$ (R_{obs} with $-h+k+l+m = 3n$) (Fig. 5). Satellite reflections are visible up to the second order (Fig. 5a,c). At 98 K and 298 K, the component of the modulation wave vector appears very close to a commensurate value. The choice of the

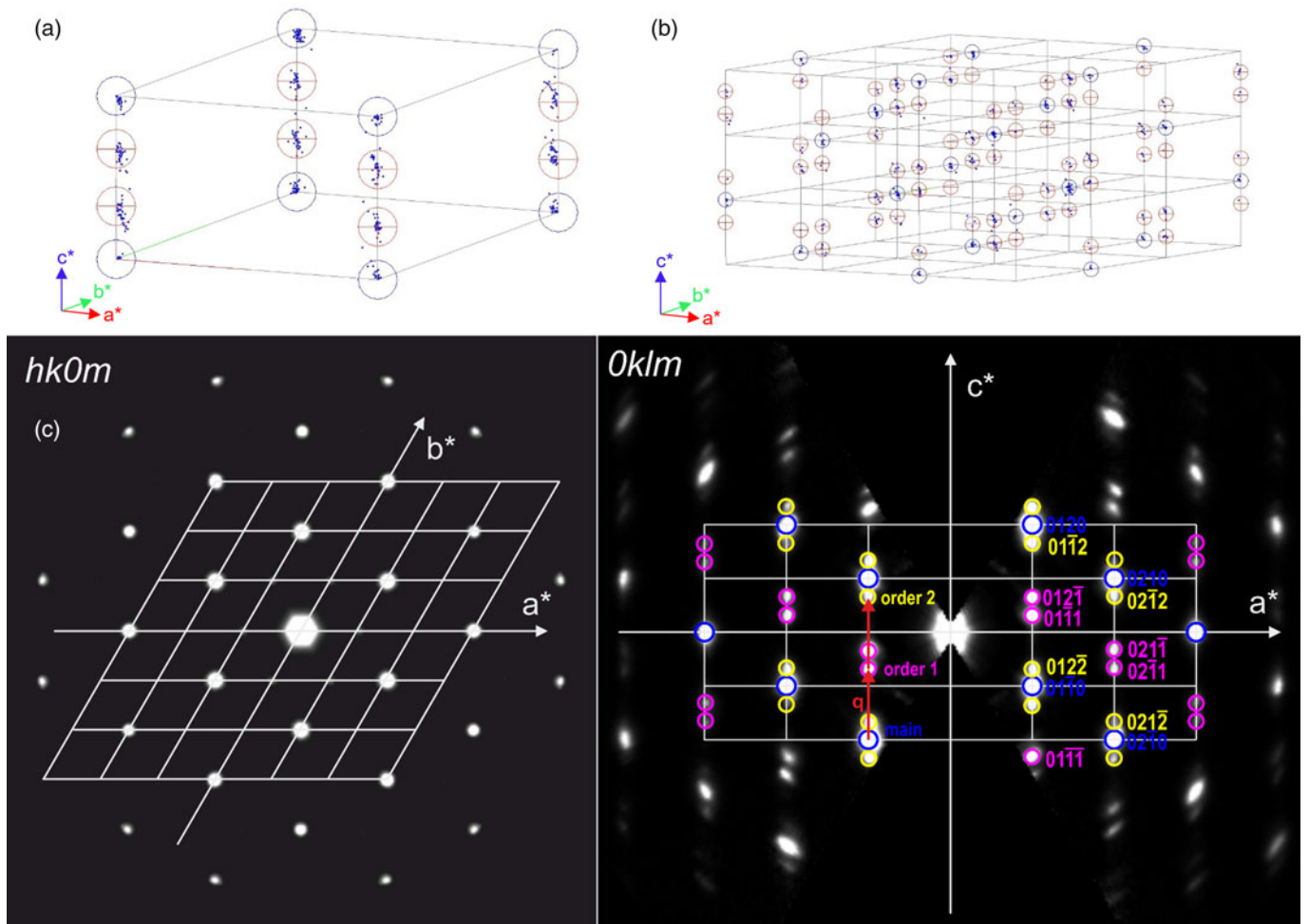


Figure 5. Indexing using the superspace (SS) formalism $a = 4.209(2)$, $c = 5.610(6)$ Å, $\mathbf{q} = 1.325(5)\mathbf{c}^*$ and $R\bar{3}m(00\gamma)00$ and represented in (a) one folded unit cell, and (b) in an extended unit cell $3a^* \times 3a^* \times 3c^*$ where the R centering is visible for main (blue) and the satellite (red) reflections (PETS2 software). (c) Sections $hk0m$ and $Oklm$ of the reciprocal space highlighting a few main (blue), first order satellite (pink), and second order (yellow) satellite reflections.

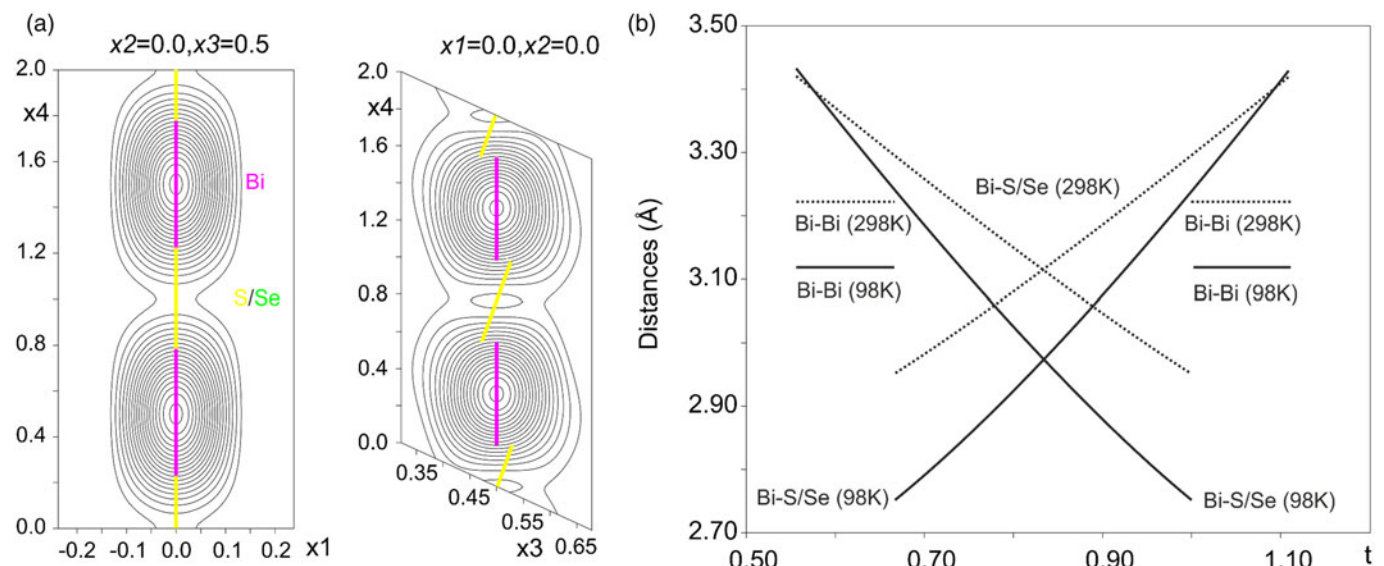


Figure 6. (a) De Wolf sections x_1 - x_4 and x_3 - x_4 drawn from $F(\text{obs})$ with Bi and S/Se domains along x_4 using crenel functions and Legendre polynomials in crenel intervals (98 K). (b) Distances Bi-Bi and Bi-S/Se along the parameter t at 98 K and 298 K. This parameter is explained in detail in the text.

Table 4. Positional parameters and atomic displacement parameters for the crystal structure of zipserite at 298 K.

Atom	Δ	x40	Occupational waves			
Bi1	0.5556	0.5				
S1/Se	0.4444	0				
Atom	Occ	Wave	x	y	z	U_{eq}/U_{iso}
Bi1	0.5555	o,1	0	0	$\frac{1}{2}$	0.0466(12)
			0	0	0.008(2)	
			0	0	0	
S1	0.3778	o,1	0	0	$\frac{1}{2}$	0.089(9)
			0	0	0.075(11)	
			0	0	0	
Se1	0.0667	o,1	0	0	$\frac{1}{2}$	0.084(3)
			0	0	0.075(11)	
Atom	U^{11}	U^{22}	U^{33}	U^{12}	U^{13}	U^{23}
Bi1	0.0330(9)	0.0330(9)	0.074(3)	0.0165(4)	0	0
S1/Se	0.039(2)	0.039(2)	0.19(3)	0.0194(12)	0	0

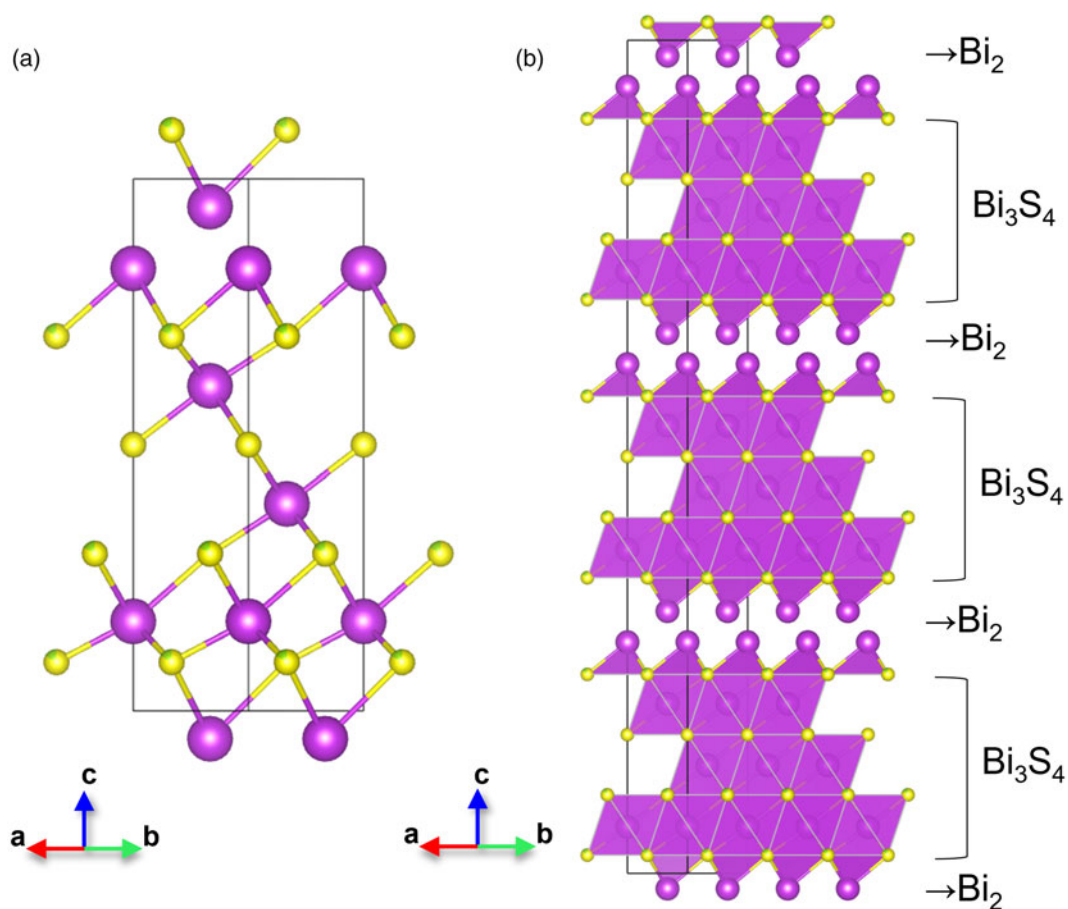
**Figure 7.** (a) Crystal structure of Bi_5S_4 (i.e. no Se considered as it is a minor element in the structure with no separate positions) represented in the supercell $a \times b \times 3c_0$ (space group $P\bar{3}m1$). (b) Bi_5S_4 represented in an extended supercell to show the stacking of Bi_2 and Bi_3S_4 layers. Drawn using *CrystalMaker*[®] software.

Table 5. Positional parameters and atomic displacement parameters for the crystal structure of zipserite at 98 K.

Occupational waves						
Atom	Δ	x40				
Bi1	0.5556	0.5				
S1/Se	0.4444	0				
Positional parameters						
Atom	Occ	Wave	x	y	z	Ueq/Uiso
Bi1	0.5555	o,1	0	0	1/2	0.0255(7)
			0	0	0.0095(14)	
			0	0	0	
S1	0.3778	o,1	0	0	1/2	0.059(9)
			0	0	0.109(8)	
			0	0	0	
Se1	0.0667	o,1	0	0	1/2	0.059(9)
			0	0	0.109(8)	
			0	0	0	
Atomic displacement harmonic parameters						
Atom	U^{11}	U^{22}	U^{33}	U^{12}	U^{13}	U^{23}
Bi1	0.0162(6)	0.0162(6)	0.0441(17)	0.0081(3)	0	0
S1/Se	0.0267(18)	0.0267(18)	0.12(3)	0.0134(9)	0	0

superspace formalism over a 3-dimensional cell with $3c_0$ ($P\bar{3}m$) was made because of the intensity repartition, and the possibility of more accurately describing the ordering between Bi and S/Se atoms. The second-order satellite reflections were involved in the structure solution but must be discarded from the refinement as their integration was found to be inaccurate (Fig. S1). The recent 'fit profile' option in *PETS2* allows better integration of close reflections. However, for zipserite, the *c*-axis, where the modulation takes place, is lying along the beam direction during

the experiment and is associated with an unusually high mosaicity.

The result of the charge flipping algorithm (*Superflip*) is a (3+1)-dimensional map of the electrostatic potential (emap) that is interpreted according to the isosurface levels ($V(r)$). The initial model has only 1 independent atomic site. The repartition of the electrostatic potential on this site along the modulation axis x_4 can be visualised on de-Wolf sections x_1-x_4 and x_3-x_4 (Fig. 6a). The model was further elaborated by splitting the domain in two using crenel functions to describe the occupational modulation between Bi and S/Se, and Legendre polynomials in crenel intervals to account for a possible positional modulation. The ordering is considered between Bi and S/Se. From the quality of the present data set, we cannot speculate on a possible additional ordering between S and Se. The first atomic site is defined with a crenel function for Bi as $x_4^0 = 0.5$, the centre of the crenel and $\Delta[\text{Bi}] = 5/9 \approx 0.556$, the width of the domain according to the chemical composition. The S/Se domain is then defined with $x_4^0 = 0$ and $\Delta[\text{S/Se}] = 1-5/9 = 4/9 \approx 0.444$. The amount of S and Se on this domain is set to agree with the result of the chemical analysis as S:Se = 85:15. The same model was obtained for the 3D ED data collected at 98 K and 298 K (Table 3). The refinements were carried out using both the kinematical and the dynamical approaches (Table 3). Imperfect crystals tend to diffract more kinematically which usually results in a smaller decrease of the *R*-factors from the kinematical to the dynamical refinement, as is the case here. However, it does not mean that the multiple scattering does not occur (dynamical diffraction), especially when heavy atoms are involved. Due to data limitations, i.e. strong mosaicity, absence of the second order in the refinement and lower data coverage along *c*, the refinements were performed using restrictions on the distances between Bi and S/Se. The displacive modulation appears correlated to the anisotropic displacement along *c*. Therefore, gentle restrictions allowed more meaningful Bi-(S/Se) distances, compared with the values found in the literature. The refinement using the dynamical and the kinematical approaches led to very close results in terms of displacement parameters.

Table 6. Calculated powder XRD data for zipserite.*

$100 \cdot I_{\text{calc}}/I_{\text{max}}$	d_{calc}	<i>h</i>	<i>k</i>	<i>l</i>
9	16.397	0	0	1
10	4.099	0	0	4
18	3.520	1	0	1
5	3.300	0	1	2
14	3.300	1	0	2
4	3.279	0	0	5
100	3.009	0	1	3
5	2.4257	1	0	5
37	2.1777	1	0	6
37	2.0810	1	1	0
4	1.9641	0	1	7
7	1.8556	1	1	4
6	1.8219	0	0	9
3	1.7914	0	2	1
3	1.7602	0	2	2
4	1.7571	1	1	5
20	1.7116	2	0	3
12	1.5045	0	2	6
3	1.4603	1	1	8
15	1.3708	1	1	9
2	1.3577	2	1	1
2	1.3439	2	1	2
17	1.3219	1	2	3
5	1.2777	0	1	12

*Intensity and d_{hkl} were calculated using the software *PowderCell2.3* (Kraus and Nolze, 1996) on the basis of the structural model given in Tables 3 and 4. Only reflections with $I_{\text{calc}} > 2$ are listed. The five strongest reflections are given in bold.

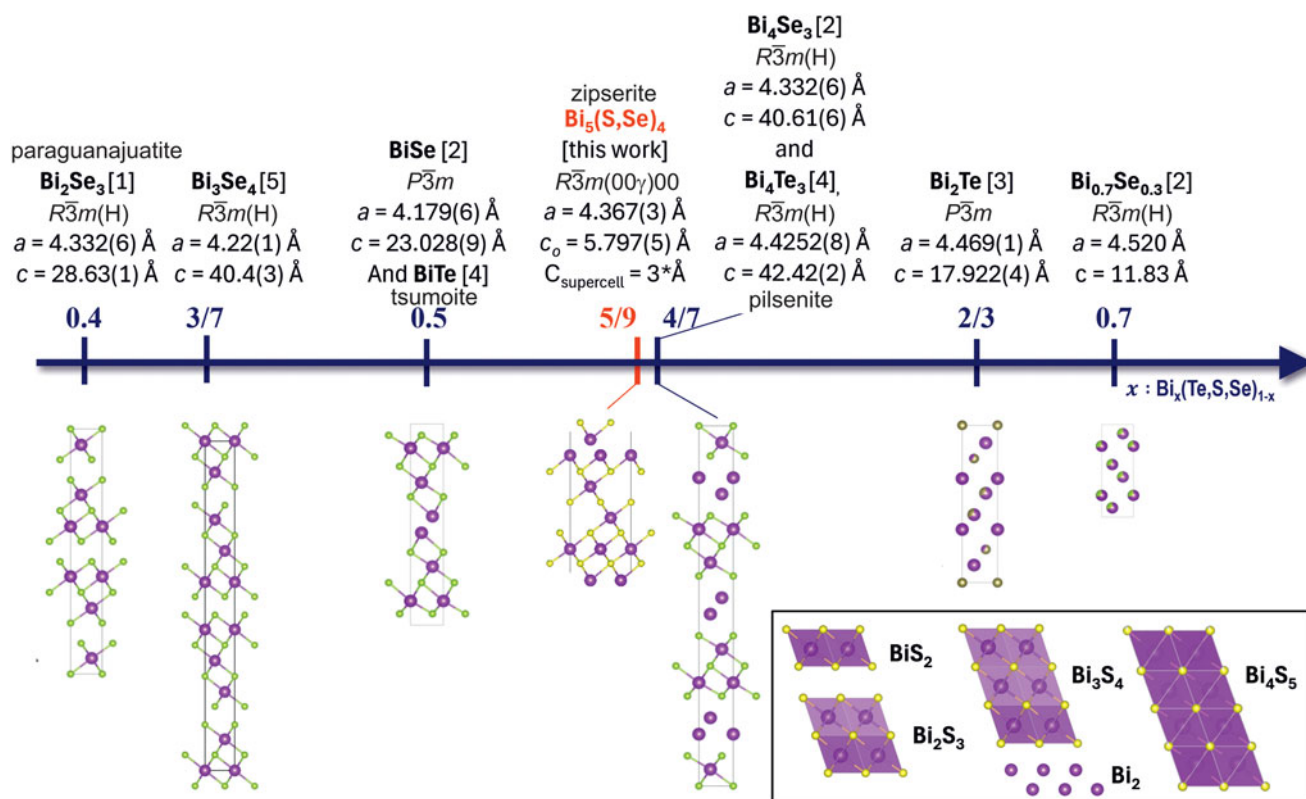


Figure 8. Scheme with related synthetic compounds sorted by their x ratio. References: [1] Nakajima (1963); [2] Gardes *et al.* (1989); [3] Yamana *et al.* (1979); [4] Glazov (1984); [5] Semiletov and Pinsker (1955). The basic structural units are presented in the insert.

The results of the dynamical refinement are nevertheless preferred as the R values improved and this refinement was performed on more reflections (Palatinus *et al.*, 2015a, 2015b; Klar *et al.*, 2023). At 98 K, the refinement converged to $R(\text{obs})/wR(\text{obs}) = 0.096/0.1185$ and $R(\text{all})/wR(\text{all}) = 0.096/0.1185$ for 768 observed reflections and 60 refined parameters including only six structural ones. At 298 K, the results are $R(\text{obs})/wR(\text{obs}) = 0.1142/0.1376$, $R(\text{all})/wR(\text{all}) = 0.1192/0.1380$ for 616 observed reflections and 47 refined parameters for six structural ones. The detail of the R values for the main and satellite reflections is given in Table 3. For $Z = 1$, the general formula is $\text{Bi}_{1.667}(\text{S}_{1.133}\text{Se}_{0.2})_{\Sigma 1.333}$ corresponding to $x = 0.556$ when the formula is expressed as $\text{Bi}_x(\text{S,Se})_{1-x}$. The Bi–Bi and Bi–S/Se distances along the parameter t at 98 K and 298 K are presented in Fig. 6b, the positional parameters and atomic displacement parameters in Tables 4 and 5, respectively. The parameter t is defined as $\bar{x}(s,4) = t + q \cdot \bar{x}(u)$, $0 < t < 1$. By construction, the fourth coordinate axis in superspace is perpendicular to physical space. The fourth coordinate $\bar{x}(s,4)$ of a point in superspace then is $\bar{x}(s,4) = t + q \cdot \bar{x}(u)$, where $\bar{x}(u)$ are the three coordinates of atom u in the basic (average) structure. The parameter t can be considered as the initial phase of the modulation wave. Different values of t give shifted, but entirely equivalent representations of physical space. For crystal structures, the variation of environments of a particular atom of the basic structure can be obtained as a function of t of structural parameters, like atomic displacements, atomic distances, bond angles, etc. The structure is shown in Fig. 7.

Powder XRD data of zipserite could not be collected, due to the paucity of available material. Consequently, powder XRD data, given in Table 6, were calculated using the software

PowderCell 2.3 (Kraus and Nolze, 1996) on the basis of the structural model given in Table 4. The crystallographic information files have been deposited with the Principal Editor of *Mineralogical Magazine* and are available as Supplementary material (see below).

Discussion

An easier way to visualise the structure is to draw the model in the closest supercell $a \times b \times 3c_0$ with formula $\text{Bi}_5(\text{S}_{3.4}\text{Se}_{0.6})_{\Sigma 4}$ (space group $P\bar{3}m$) (Fig. 7). $\text{Bi}_5(\text{S}_{3.4}\text{Se}_{0.6})_{\Sigma 4}$ is built from the alternation of the double bismuth layer Bi_2 and the Bi_3S_4 block which is a three Bi_6 octahedra thick layer. Its general formula can be expressed as $\text{Bi}_2 + \text{Bi}_3\text{S}_4$, which corresponds directly to the observed stacking. For both temperatures, the Bi–Bi distances are constant along the modulation with Bi–Bi = 3.118(7) Å at 98 K, and Bi–Bi = 3.221(11) Å at 298 K and correspond to the double bismuth layer. In the Bi_3S_4 block, bismuth atoms are not located at the centre of the octahedra formed by neighbouring S/Se atoms. The refined positional modulation parameter for bismuth (*zort1*) is almost zero whereas the values go up to 0.109(8) for S/Se at 98 K and 0.0745(11) at 298 K. This is illustrated by the variation of Bi–S/Se distances along the domain which is only due to a significant displacement of S/Se along c (Fig. 6b). The longest Bi–S/Se distances are found between the Bi_2 double layer, and the first S/Se positions. This result is totally consistent with what is observed in the $(\text{Bi}_2)_m(\text{Bi}_2\text{Te}_3)_n$ system (Bos *et al.*, 2012). The temperature induces a difference in the modulation amplitudes, where lower temperature data show a stronger evolution of the Bi–S/Se distances (from 2.76(3) Å to 3.43(3) Å at 98 K, and

from 2.95(4) Å to 3.42(4) Å at 298 K). Note that the difference observed for the modulation parameters might be a bit inflated by the lower coverage of the data at 98 K (81.92%) as compared to the data collected at the ambient temperature. Nevertheless, the Bi atoms, being part of the Bi_3S_4 blocks, are shifted significantly from the exact central position defined by the surrounding S/Se atoms. Such a feature has already been observed for compounds of the same family (Fig. 8). This scheme only includes binary compounds, but many more doped materials exist (Aliiev *et al.*, 2019), allowing more complex stackings. Bos *et al.* (2012) described the structure and the properties of the $(\text{Bi}_2)_m(\text{Bi}_2\text{Te}_3)_n$ natural superlattices synthesised with compositions $\text{Bi}_x\text{Te}_{1-x}$ with $0.44 \leq x \leq 0.70$. They found an infinitely adaptive series of layered $(\text{Bi}_2)_m$ and $(\text{Bi}_2\text{Te}_3)_n$ (2-octahedra thick) natural superlattices consisting of different stacking sequences of Bi double layers and Bi_2Te_3 blocks. In Fig. 8, several examples of fully ordered and disordered structures are shown. The stacking of all ordered structures can be derived through their composition by decomposing the nominal composition into not only $(\text{Bi}_2)_m$ and $(\text{Bi}_2\text{Te}_3)_n$ but a flexible combination of $(\text{Bi}_2)_m$, $(\text{BiTe}_2)_n$, $(\text{Bi}_2\text{Te}_3)_o$, $(\text{Bi}_3\text{Te}_4)_p$, and so on (see the insert in Fig. 8). BiSe stacking can be determined as $[2^*\text{Bi}_2\text{S}_3 + \text{Bi}_2]$ (Gardes *et al.*, 1989). In the system Bi–Te for $x = 2/3$ and $(\text{Bi}_2\text{Te}_3)_n$ for $x = 0.7$, the structures are disordered (Glazov *et al.*, 1984; Yamana *et al.*, 1979) as their formula cannot be decomposed into a series of basic structural units. Moreover, the refinement of zipserite in the commensurate option did not lead to good results. It suggests that the component of modulation wave vector is not exactly $4/3$ for $x = 0.556$ and can probably evolve with the composition. We can presume that zipserite can show some structural flexibility to accommodate chemical variations (particularly S/Se ratio) depending on the available elements in the geological environment. It could be present under a slightly different combination of $(\text{Bi}_2)_m$ and $(\text{Bi}_3\text{S}_4)_p$, maybe as even more complex, uneven stacking of blocks $[(\text{Bi}_2\text{S}_3)_o + (\text{Bi}_4\text{S}_5)_q]$ such as for systems where Bi is doped with other elements like MnBi_4Te_4 or $\text{MnBi}_6\text{Te}_{10}$ (Aliiev *et al.*, 2019).

Following the results of the crystal structure analysis of zipserite (occupation of 2c site $\text{Se}_{0.41}\text{S}_{0.35}\text{Bi}_{0.24}$), its ideal formula could be written as $\text{Bi}_5\text{S}_2\text{Se}_2$ (Nickel and Grice, 1998). However, difficulties related to the refinement of the zipserite structure and the measured (using electron probe microanalysis) Se contents of only 0.56 apfu leave some questions regarding the exact composition open. For nomenclature purposes, we propose that the 2c and 2d sites should be considered as an aggregate site, avoiding the creation of different isotopes of zipserite based on different S/Se ratios. Thus, species with $\text{S} > \text{Se}$ should be classified as zipserite, and those with $\text{Se} > \text{S}$ could be described as a potential new mineral species.

Conclusions

Zipserite is a new phase in the Bi–S(–Se) system related to the tetradymite archetype (Cook *et al.*, 2007) and it does not correspond to any valid or invalid unnamed mineral of Smith and Nickel (2007). Its discovery and comparison with previously known Bi chalcogenides confirm the fundamental role of studies devoted to natural mineral assemblages to reveal novel crystal structures so far not synthesised in a laboratory (e.g. Gardes *et al.*, 1989; Lin *et al.*, 1996; Kitakaze, 2016, 2017; Bindi *et al.*, 2020).

Acknowledgements. We appreciate the constructive comments of three anonymous reviewers and the editorial handling by Owen Missen. GS wants

to thank Lukáš Palatinus for the extra brain cells as well the CzechNanoLab project LM2023051 funded by MEYS CR for the financial support of the measurements/sample fabrication at LNSM Research Infrastructure. This work is also supported by the Czech Science Foundation, project number 21-05926X. JS acknowledges financial support by the Ministry of Culture of the Czech Republic (long-term project DKRVO 2024–2028/1.II.a; National Museum, 00023272).

Supplementary material. The supplementary material for this article can be found at <https://doi.org/10.1180/mgm.2024.37>.

Competing interests. The authors declare that they have no known competing financial interests or personal relationships that could have appeared to influence the work reported in this paper.

References

- Aliiev Z.S., Amiraslanov I.R., Nasonova D.I., Shevelkov A.V., Abdullayev N.A., Jahangirli Z.A., Orujlu E.N., Otrokov M.M., Mamedov N.T., Babanly M.B. and Chulkov E.V. (2019) Novel ternary layered manganese bismuth tellurides of the $\text{MnTe–Bi}_2\text{Te}_3$ system: Synthesis and crystal structure. *Journal of Alloys and Compounds*, **789**, 443–450.
- Bezák V., Bielik M., Marko F., Zahorec P., Pašteka R., Vozár J. and Papčo J. (2023) Geological and tectonic interpretation of the new Bouguer gravity anomaly map of Slovakia. *Geologica Carpathica*, **74**, 109–122.
- Bindi L., Nespolo M., Krivovichev S.V., Chapuis G. and Biagioni C. (2020) Producing highly complicated materials. Nature does it better. *Reports on Progress in Physics*, **83**, 106501.
- Bindi L., Keutsch F.N., Topa D., Kolitsch U., Morana M. and Tait K.T. (2023) First occurrence of the $M2a2b2c$ polytype of argentopolybasite, $[\text{Ag}_6\text{Sb}_2\text{S}_7][\text{Ag}_{10}\text{S}_4]$: Structural adjustments in the Cu-free member of the pearceite–polybasite group. *Mineralogical Magazine*, **87**, 561–567.
- Bos J.W.G., Faucheu F., Downie R.A. and Marcinkova A. (2012) Phase stability, structures and properties of the $(\text{Bi}_2)_m(\text{Bi}_2\text{Te}_3)_n$ natural superlattices. *Journal of Solid State Chemistry*, **193**, 13–18.
- Brázda P., Klementová M., Krysiak Y. and Palatinus L. (2022) Accurate lattice parameters from 3D electron diffraction data. I. Optical distortions. *IUCrJ*, **9**, 1–21.
- Cook N.J., Ciobanu C.L., Wagner T. and Stanley C.J. (2007) Minerals of the system Bi–Te–Se–S related to the tetradymite archetype: review of classification and compositional variation. *The Canadian Mineralogist*, **45**, 665–708.
- Gardes B., Brun G. and Tedenac J.C. (1989) Contribution to the study of the bismuth–selenium system. *European Journal of Solid State and Inorganic Chemistry*, **26**, 221–229.
- Gemmi M. and Lanza A.E. (2019) 3D electron diffraction techniques. *Acta Crystallographica*, **B75**, 495–504.
- Gemmi M., Mugnaioli E., Gorelik T.E., Kolb U., Palatinus L., Boullay P., Hovmöller S. and Abrahams J.P. (2019) 3D electron diffraction: The nanocrystallography revolution. *ACS Central Science*, **5**, 1315–1329.
- Glazov V.M. (1984) Production of semiconducting materials by the method of ultrafast cooling of the melt. *Inorganic Materials*, **20**, 1068–1074.
- Heremans J.P., Cava R.J. and Samarth N. (2017) Tetradymites as thermoelectrics and topological insulators. *Nature Reviews Materials*, **2**, 17049.
- Hurai V., Huraiová M., Nemeč O., Konečný P. and Reato L. (2023) Systematics of clinopyroxene phenocrysts, megacrysts, and cumulates in Tertiary basalts of southern Slovakia with implications in the structure of lithospheric mantle. *Geologica Carpathica*, **74**, 325–346.
- Kitakaze A. (2016) Phase relation of some sulfide systems-(2). *Memoirs of the Faculty of Engineering, Yamaguchi University*, **67**, 19–33.
- Kitakaze A. (2017) Phase relation of some sulfide systems-(3). *Memoirs of the Faculty of Engineering, Yamaguchi University*, **68**, 1–31.
- Klar P.B., Krysiak Y., Xu H., Steciuk G., Cho J., Zou X., Palatinus L. and Republic C. (2023) Accurate structure models and absolute configuration determination using dynamical effects in continuous-rotation 3D ED data. *Nature Chemistry*, **15**, 848–855, <https://doi.org/10.1038/s41557-023-01186-1>.
- Koch S. and Grasselly G. (1952) The minerals of the sulphide ore-deposit of Nagyborzsöny. *Acta Mineralogica-Petrographica*, **6**, 1–21.

- Kraus W. and Nolze G. (1996) POWDER CELL – a program for the representation and manipulation of crystal structures and calculation of the resulting X-ray powder patterns. *Journal of Applied Crystallography*, **29**, 301–303.
- Kuribayashi T., Nagase T., Nozaki T., Ishibashi J., Shimada K., Shimizu M. and Momma K. (2019) Hitachiite, $\text{Pb}_5\text{Bi}_2\text{Te}_2\text{S}_6$, a new mineral from the Hitachi mine, Ibaraki Prefecture, Japan. *Mineralogical Magazine*, **83**, 733–739.
- Lin J.C., Sharma R.C. and Chang Y.A. (1996) The Bi-S (bismuth-sulfur) system. *Journal of Phase Equilibria*, **17**, 132–139.
- Majzlan J., Ozdín D., Sejkora J., Steciuk G., Plášil J., Rößler C. and Matthes C. (2022) Zipserite, IMA 2022-075. CNMNC Newsletter 70, *Mineralogical Magazine*, **87**, 164–165, <https://doi.org/10.1180/mgm.2022.135>
- Nakajima S. (1963) The crystal structure of $\text{Bi}_2\text{Te}_{3-x}\text{Se}_x$. *Journal of Physics and Chemistry of Solids*, **24**, 479–485.
- Nickel E.H. and Grice J.D. (1998) The IMA Commission on New Minerals and Mineral Names: procedures and guidelines on mineral nomenclature, 1998. *The Canadian Mineralogist*, **36**, 913–926.
- Paar W.H., Putz H., Topa D., Roberts A.C., Stanley C.H.J. and Culetto F.J. (2006) Jonassonite, $\text{Au}(\text{Bi,Pb})_5\text{S}_4$, a new mineral species from Nagybörzsöny, Hungary. *The Canadian Mineralogist*, **44**, 1127–1136.
- Palatinus L. (2013) The charge-flipping algorithm in crystallography. *Acta Crystallographica*, **B69**, 1–16.
- Palatinus L. and Chapuis G. (2007) SUPERFLIP – A computer program for the solution of crystal structures by charge flipping in arbitrary dimensions. *Journal of Applied Crystallography*, **40**, 786–790.
- Palatinus L., Corrêa C.A., Steciuk G., Jacob D., Roussel P., Boullay P., Klementová M., Gemmi M., Kopeček J., Domeneghetti M.C., Cámara F. and Petříček V. (2015a) Structure refinement using precession electron diffraction tomography and dynamical diffraction: tests on experimental data. *Acta Crystallographica*, **B71**, 740–751.
- Palatinus L., Petříček V. and Corrêa C.A. (2015b) Structure refinement using precession electron diffraction tomography and dynamical diffraction: Theory and implementation. *Acta Crystallographica*, **A71**, 235–244.
- Palatinus L., Brázda P., Jelínek M., Hrdá J., Steciuk G. and Klementová M. (2019) Specifics of the data processing of precession electron diffraction tomography data and their implementation in the program PETS2.0. *Acta Crystallographica*, **B75**, 512–522.
- Pantó G. and Mikó L. (1964) Minerals of Nagybörzsöny. *Annales Instituti Geologici Publici Hungarici*, **50**, 1–153 [in Hungarian].
- Pathak R., Dutta P., Srivastava A., Rawat D., Gopal R.K., Singh A.K., Soni A. and Biswas K. (2022) Strong anharmonicity-induced low thermal conductivity and high n-type mobility in the topological insulator $\text{Bi}_{1.1}\text{Sb}_{0.9}\text{Te}_2\text{S}$. *Angewandte Chemie – International Edition*, **61**, e202210783.
- Pauling L. (1975) The formula, structure, and chemical bonding of tetradymite, $\text{Bi}_{14}\text{Te}_{13}\text{S}_8$, and the phase $\text{Bi}_{14}\text{Te}_{15}\text{S}_6$. *American Mineralogist*, **60**, 994–997.
- Petříček V., Palatinus L., Plášil J. and Dušek M. (2023) Jana2020 - a new version of the crystallographic computing system Jana. *Zeitschrift für Kristallographie*, **238**, 271–282.
- Sejkora J., Biagioni C., Škácha P. and Mauro D. (2023a) Vrančiceite, $\text{Cu}_{10}\text{Hg}_3\text{S}_8$, a new Cu–Hg sulfide mineral from Vrančice, Czech Republic. *Mineralogical Magazine*, **87**, 670–678.
- Sejkora J., Biagioni C., Škácha P., Musetti S., Kasatkin A.V. and Nestola F. (2023b) Tetrahedrite-(Cd), $\text{Cu}_6(\text{Cu}_4\text{Cd}_2)\text{Sb}_4\text{S}_{13}$, from Radětice near Příbram, Czech Republic: the new Cd member of the tetrahedrite group. *European Journal of Mineralogy*, **35**, 897–907.
- Semiletov S.A. and Pinsker Z.G. (1955) The electron diffraction analysis of the system of alloys Bi–Se. *Doklady Akademii Nauk SSSR*, **100**, 1079–1082.
- Smith D.G.W. and Nickel E.H. (2007) A system for codification for unnamed minerals: report of the Subcommittee for Unnamed Minerals of the IMA Commission on New Minerals, Nomenclature and Classification. *The Canadian Mineralogist*, **45**, 983–1055.
- Szakáll S. (editor) (2002) *Minerals of the Carpathians*. Granit, Prague, 479 pp.
- Szakáll S., Zajzon N. and Kristály F. (2012) Unusual ikunolite from Nagybörzsöny ore deposit, Börzsöny, Mts., Hungary. *Acta Mineralogica-Petrographica, Abstract Series*, **7**, 134.
- Yamana K., Kihara K. and Matsumoto T. (1979) Bismuth tellurides: BiTe and Bi_4Te_3 . *Acta Crystallographica*, **B35**, 147–149.
- Yamini S.A., Santos R., Fortulan R., Gazder A.A., Malhotra A., Vashae D., Serhienko I. and Mori T. (2023) Room-temperature thermoelectric performance of n-type multiphase pseudobinary Bi_2Te_3 - Bi_2S_3 compounds: synergic effects of phonon scattering and energy filtering. *ACS Applied Materials & Interfaces*, **15**, 19220–19229.